

ORIGINAL ARTICLE

Dedifferentiation into blastomere-like cancer stem cells via formation of polyploid giant cancer cells

N Niu, I Mercado-Uribe and J Liu

Our recent perplexing findings that polyploid giant cancer cells (PGCCs) acquired embryonic-like stemness and were capable of tumor initiation raised two important unanswered questions: how do PGCCs acquire such stemness, and to which stage of normal development do PGCCs correspond. Intriguingly, formation of giant cells due to failed mitosis/cytokinesis is common in the blastomere stage of the preimplantation embryo. However, the relationship between PGCCs and giant blastomeres has never been studied. Here, we tracked the fate of single PGCCs following paclitaxel-induced mitotic failure. Morphologically, early spheroids derived from PGCCs were indistinguishable from human embryos at the blastomere, polyploid blastomere, compaction, morula and blastocyst-like stages by light, scanning electron or three-dimensional confocal scanning microscopy. Formation of PGCCs was associated with activation of senescence, while budding of daughter cells was associated with senescence escape. PGCCs showed time- and space-dependent activation of expression of the embryonic stem cell markers OCT4, NANOG, SOX2 and SSEA1 and lacked expression of Xist. PGCCs acquired mesenchymal phenotype and were capable of differentiation into all three germ layers *in vitro*. The embryonic-like stemness of PGCCs was associated with nuclear accumulation of YAP, a key mediator of the Hippo pathway. Spheroids derived from single PGCCs grew into a wide spectrum of human neoplasms, including germ cell tumors, high-grade and low-grade carcinomas and benign tissues. Daughter cells derived from PGCCs showed attenuated capacity for invasion and increased resistance to paclitaxel. We also observed formation of PGCCs and dedifferentiation in ovarian cancer specimens from patients treated with chemotherapy. Taken together, our findings demonstrate that PGCCs represent somatic equivalents of blastomeres, the most primitive cancer stem cells reported to date. Thus, our studies reveal an evolutionarily conserved archaic embryonic program in somatic cells that can be de-repressed for oncogenesis. Our work offers a new paradigm for cancer origin and disease relapse.

Oncogene (2017) 36, 4887–4900; doi:10.1038/onc.2017.72; published online 24 April 2017

INTRODUCTION

A hallmark of many malignant tumors is dedifferentiated (immature) cells bearing little or no resemblance to the normal cells from which the cancer originated.¹ A salient feature of dedifferentiation is the presence of giant cells with multiple copies of genomic DNA, referred to as polyploid giant cancer cells (PGCCs).² A polyploid genome has been found in 37% of solid tumors.³

Polyploid cells were traditionally considered senescent and induction of polyploidy was traditionally considered a tumor suppressor mechanism as polyploid cells are believed to be unable to execute mitosis.^{4–7} However, PGCCs have been shown to generate daughter cells via budding^{8–12} and to contribute to immortalization, transformation and RAS-mediated tumor initiation and metastasis.^{13–15} Furthermore, tetraploid cells, not diploid cells, have been shown to be the main drivers of tumorigenesis.^{16,17} In addition, development of polyploidy has been shown to favor escape from senescence in chemotherapy-treated cancer cells.^{18–20} However, the mechanisms by which polyploidy gives rise to malignancy remain poorly defined.

We recently reported that PGCCs are cancer stem cells that can be induced from ovarian cancer cells by the hypoxia-mimetic agent CoCl₂.² We showed that PGCCs from ovarian cancer can grow into tumor spheroids, initiate tumor growth in nude mice

and differentiate into other benign cell types *in vitro* and *in vivo*.^{2,14,21,22} These properties of PGCCs were also reported in colon cancer.²³ A PGCC phenotype has recently been linked to CSL, a central node in Notch signaling.²⁴ We also showed that growth and division of PGCCs involves a multistep programmed process, which we refer as to the giant cell cycle, with four distinct but overlapping phases, initiation, self-renewal, termination and stability, via which PGCCs give rise to new cancer-initiating cells.²⁵ However, it is unclear how PGCCs acquire such stemness and which normal developmental stage PGCCs correspond to.

Polyploidy is common in plants and nonvertebrate animals but is generally incompatible with normal development of mammals except in a limited number of somatic cells or tissues.^{4,26,27} Intriguingly, blastomeres, which are produced by cleavage of the zygote in the human preimplantation embryo, frequently display mosaicism of diploidy and polyploidy. As embryogenesis progresses, mononucleated or multinucleated giant blastomeres are commonly seen due to frequent mitosis/cytokinesis failure and endoreplication.^{28–32} The proportion of embryos with more than five polyploid cells is 30.8% for morulae and 29.3% for blastocysts.³³ A large proportion of polyploid blastomeres (50–80%) display high levels of genomic abnormalities.^{29–31,34–36} Therefore, formation of polyploid blastomeres appears to facilitate the development of compaction and subsequent blastocysts, and

mitosis/cytokinesis failure may represent a normal mechanism regulating development of the preimplantation embryo.^{28,29,37}

The similarities between PGCCs and blastomeres raise the intriguing possibility that PGCCs are somatic equivalents of blastomeres. To investigate this possibility, we tracked the development of single PGCCs derived from ovarian cancer cells treated with paclitaxel.

RESULTS

PGCCs exhibited a developmental pattern similar to that of the blastomere-like embryo

The experimental design is shown in Figure 1A. Ovarian cancer cell lines Hey, SKOV3 and MDA-HGSC-1 were treated with paclitaxel overnight (16–18 h) to induce mitotic failure. The surviving cells entered an endoreplication cell cycle, grew as PGCCs and were allowed to recover for 7 days as previously described.²⁵ At day 7 (spheroid day 1 (sD1)), PGCCs were collected for three-dimensional (3D) culture or transferred to stem cell medium and allowed to grow as spheroids. From sD1 to sD21, spheroids were collected at different time points and fixed for immunofluorescence and immunohistochemical staining (IHC). At sD14, spheroids were reattached on cover slides and cultured with differentiation medium for an additional 14 days. At sD28, cell differentiation was evaluated via immunofluorescence and IHC.

At sD1, light microscopy showed that paclitaxel-treated Hey and SKOV3 cells grew as homogeneous PGCCs, and paclitaxel-treated MDA-HGSC-1 cells grew as spheroids with enlarged cells (Supplementary Figure 1A). The percentage of polyploid cells was significantly higher in paclitaxel-treated than in control cells (Supplementary Figure 1B). The percentage of senescent cells was significantly higher in PGCCs than in control cells or PGCC-derived daughter cells (Supplementary Figures 1C and D). At sD7, PGCCs showed greater spheroid-forming capacity (Figure 1B) but formed smaller spheroids than control cells (Figure 1C). Representative photos of spheroids are shown in Figure 1D.

To study the development of PGCCs, growth of single control Hey cells and Hey-derived PGCCs in stem cell medium was tracked by light microscopy. Control Hey cells formed coral-like structures within 7–14 days (Figure 1E). Scanning electron microscopy showed long microvilli, ruffles and filopodia on the surface of Hey cells and Hey-derived spheroids (Figure 1F).

In contrast, Hey-derived PGCCs showed vacuolation of the cytoplasm (Figure 1G, white arrow). At sD3 and sD5, daughter cells budded from PGCCs asymmetrically, and at sD7 and sD14, spheroids were observed with mixed giant and small cells (Figure 1G). Nuclei of different sizes were found inside and on the surface of PGCCs (Figure 1H). Similar growth and morphology were seen in MDA-HGSC-derived PGCCs (Supplementary Figure 1E).

To visualize ultrastructural morphology during PGCC growth, we reattached individual Hey-derived PGCCs to ultra-low-attachment plates and tracked PGCC division by scanning electron microscopy. Unexpectedly, when PGCCs started to divide, they were covered by numerous uniform microvilli and were morphologically indistinguishable from blastomeres (Figure 1I).^{38,39} The cleavage dividing PGCCs resembled one-cell, two-cell, three-cell, four-cell, six-cell, compaction-like and 10- to 12-cell blastomeres and morulas (Figure 1I), similar to what is observed in the embryoid body.⁴⁰ On 3D confocal scanning microscopy, single PGCCs formed blastocyst-like structures (Figure 1J, Supplementary Movies 1 and 2). 3D confocal scanning images of daughter cells from PGCCs are shown in Supplementary Figure 1F and Supplementary Movie 3. We concluded that PGCCs may undergo dedifferentiation toward embryo-like structures.

PGCCs exhibited expression of embryonic stem cell markers

We next performed immunofluorescence staining to determine the expression pattern of four stem cell transcription factors, OCT4, stage-specific embryonic antigen 1 (SSEA1), SOX2 and NANOG, over 14 days in Hey-derived PGCCs transferred to serum-free stem cell medium in ultra-low-attachment dishes on sD1. SSEA1 expression in PGCCs was activated on sD1, limited to the subnuclei or cytoplasm at sD7 and decreased by sD14 (Figure 2a). OCT4 expression was activated on day sD3 and remained activated in a subset of PGCC nuclei at sD14. SOX2 expression and NANOG expression were activated on sD1 and remained activated in a subset of PGCCs at sD14.

Hematoxylin–eosin staining showed that cells in 'spheroids' derived from regular cancer cells (control spheroids) were relatively homogeneous in size (Figure 2b). In contrast, the cells in PGCC-derived spheroids exhibited marked variation in size, and PGCC-derived spheroids had anaplastic nuclei (Figure 2b, black arrows), several cyst-like structures (middle panel) and erythrocyte-like (red arrow) and macrophage-like morphology (blue arrow), suggesting that PGCC-derived spheroids were capable of dedifferentiation *in vitro*.

Notably, expression of the epithelial marker cytokeratin was significantly lost in PGCC-derived spheroids compared with control spheroids (Figure 2c), whereas expression of the mesenchymal marker fibronectin showed the opposite pattern. Consistent with the immunofluorescence results, strong OCT4 expression was found in rare cells in PGCC-derived spheroids (Figure 2c).

Next, we examined OCT4, NANOG, SOX2 and SOX4 expression in control spheroids and PGCC-derived spheroids from MDA-HGSC-1 cells (Figure 2d). Expression of all three factors was increased in PGCCs. Interestingly, the budded daughter cells were also positive for SSEA1 (Figure 2d).

Another recognized feature of embryonic stemness is loss of Xist expression, an RNA marker for inactivation of X chromosome.⁴¹ Xist expression was lost in PGCCs derived from Hey and MDA-HGSC-1 cells and was re-acquired by PGCC-derived daughter cells (Figure 2e), further supporting the acquisition of embryonic-like stemness in PGCCs.

At the messenger RNA (mRNA) level, expression of OCT4, NANOG and DAZL (deleted in azoospermia-like), a marker for primordial germ cell development,⁴² increased in paclitaxel-treated Hey and SKOV3 cells in a time-dependent manner (Figure 2f). Western blotting showed that OCT4 and NANOG expression in Hey-derived PGCCs was upregulated from sD1, peaked at sD14, when PGCCs began to bud and had almost disappeared by sD21 (Figure 2g). SOX2 expression in Hey-derived PGCCs was upregulated from sD7, peaked at sD14 and then slightly decreased sD21, when the daughter cells start to appear. Similar patterns of expression were observed in SKOV3-derived PGCCs.

Examination of expression of cancer stem cell markers ALDH1, CD133 and CD117 using fluorescence-activated cell sorting showed that ALDH1-FITC expression was higher in Hey-derived PGCCs than in regular cancer cells (Supplementary Figures 2A and B). No CD133 or CD117 expression was detected in Hey-derived PGCCs or regular cancer cells (Supplementary Figure 2C), suggesting that expression of cancer stem markers is associated with formation of PGCCs.

PGCCs can differentiate into three germ layers *in vitro*

To further determine the nature of PGCC-mediated stemness, we examined the phenotype of PGCCs following paclitaxel treatment. The cultures displayed mixtures of PGCCs and budded daughter cells of various morphologies (Figure 3A), including epithelium-like (Figure 3A(b)), fibroblast-like (Figure 3A(c)), mixed epithelial and mesenchymal (Figure 3A(d)), neuron-like (Figure 3A(e)) and very small spore-like (yeast-like) cells (Figure 3A(f)), suggesting that PGCCs are capable of differentiation into multiple lineages of daughter cells.

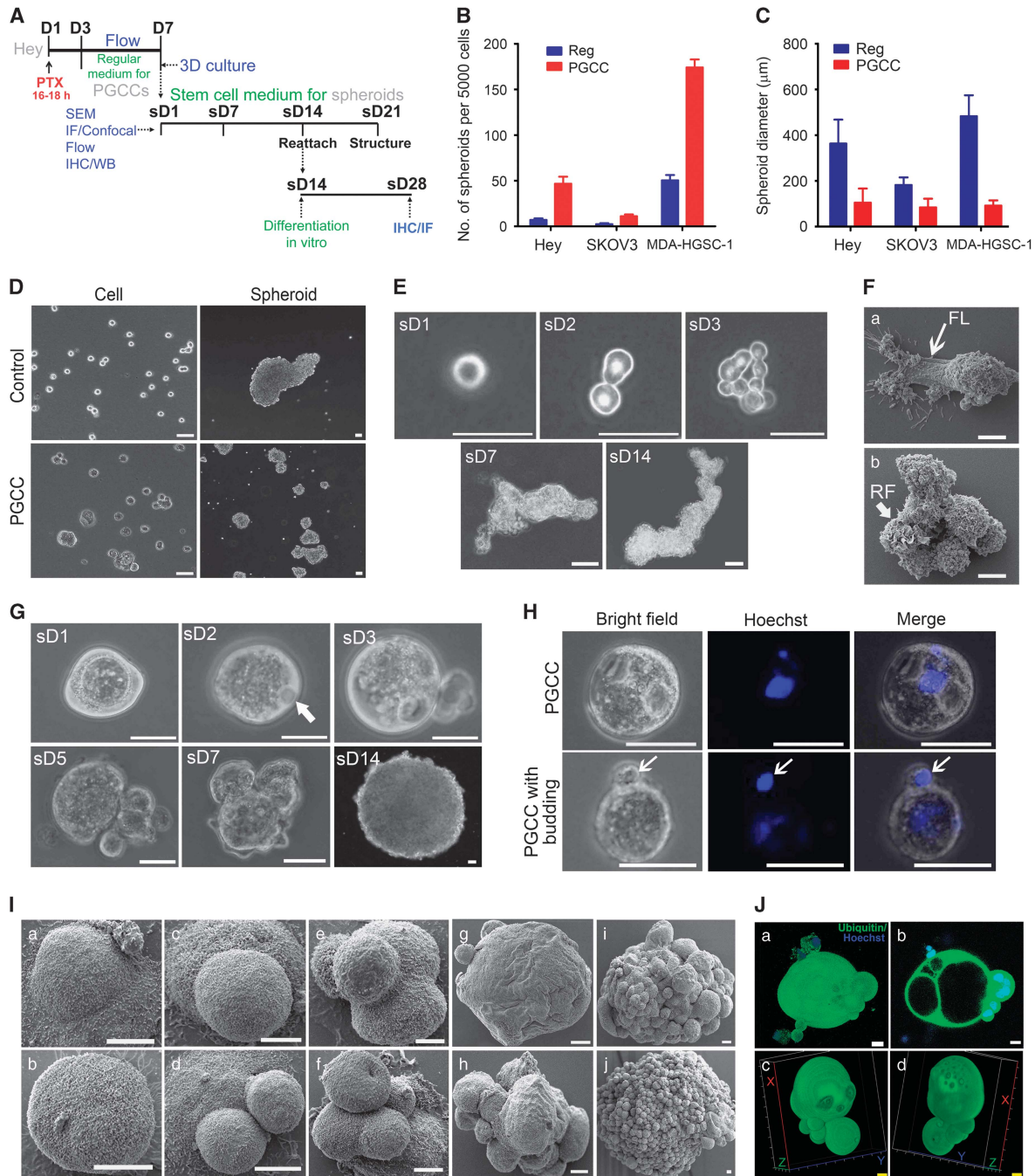


Figure 1. PGCCs exhibited a developmental pattern similar to that of blastomeres. **(A)** Experimental design. D, day; SEM, scanning electron microscopy; WB, western blotting; IF, immunofluorescence; IHC, immunohistochemistry; sD, scanning day. **(B)** Number (mean ± s.d.) of regular cancer-cell-derived spheroids and PGCC-derived spheroids per 5000 cells at sD7. Regular cancer-cell-derived spheroids: Hey, 7 ± 1.7 ; SKOV3, 2.3 ± 1.2 ; MDA-HGSC-1, 50.3 ± 5.9 . PGCC-derived spheroids: Hey, 46.7 ± 7.8 ; SKOV3, 11 ± 2 ; MDA-HGSC-1, 174.0 ± 8.8 . **(C)** Diameter (mean ± s.d.) of regular cancer-cell-derived spheroids (Hey, 363.0 ± 94.5 ; SKOV3, 182.5 ± 32.9 ; MDA-HGSC-1, 482.5 ± 91.5) and PGCC-derived spheroids (Hey, 104.2 ± 62.0 ; SKOV3, 84.0 ± 37.0 ; MDA-HGSC-1, 92.5 ± 22.5) at sD7. **(D)** Light microscopic images of control regular Hey cells, Hey-derived PGCCs and resulting spheroids at sD7. Scale bars, 50 µm. **(E)** Light microscopic images of 'spheroid' formed from a single regular Hey cell (20 µm in diameter) in serum-free stem cell medium. Scale bars, 50 µm. **(F)** Scanning electron microscopy images of regular Hey cell under mitosis (a) and spheroid derived from regular Hey cell (b). FL, filopodium; RF, ruffle. Scale bars, 10 µm. **(G)** Light microscopic images of spheroid formation from a single Hey-derived PGCC. Vacuole in the cytoplasm of PGCC is indicated with white arrowhead in panel sD2. The vacuolation is probably due to accumulation of autophagosomes. Scale bars, 50 µm. **(H)** Light microscopic nuclear morphology and size of PGCC and PGCC-derived spheroid with budding. Hoechst 33342 stain. Scale bars, 50 µm. **(I)** Scanning electron microscopy images of Hey-derived PGCCs. (a and b) PGCC mimicking single polyloid blastomere. (c–j) PGCC cleavage division mimicking blastomere division, including two-cell (c), three-cell (d), four-cell (e), six-cell (f), compaction-like (g), PGCCs with multiple small cleaved daughter cells resembling a morula (h–j). Scale bars, 10 µm. **(J)** 3D confocal scanning images of Hey-derived PGCC (a and b) and spheroid derived from Hey-derived PGCC (c and d). (a and b) Blastocyst-like PGCC with budding (a) and cross-sectional view of panel a showing multiple nuclei in a single PGCC (b). Scale bars, 100 µm. (c and d) front (c) and back (d) views of PGCC-derived spheroid. Scale bars, 10 µm.

Next, we investigated the kinetics of activation of expression of alpha fetal protein (AFP), smooth muscle actin (SMA) and β -tubulin (also known as PAX6), markers for endoderm, mesoderm and ectoderm, respectively, in Hey and SKOV3 cells. In Hey cells, mRNA levels of AFP and SMA were increased starting on day 1 of paclitaxel treatment, peaked at day 21 and decreased at day 28, by which time PGCC-derived daughter cells had formed (Figure 3B). In contrast, the mRNA levels of PAX6 remained relatively unchanged over this period. The protein levels of these three markers were much higher in Hey-derived PGCCs than in regular Hey cells and higher in daughter cells than in regular Hey cells (Figure 3C). SMA and β -tubulin protein levels were higher in SKOV3-derived PGCCs than in regular SKOV3 cells and daughter cells (Figure 3C). However, there was no change in AFP expression at the mRNA or protein level in SKOV3 cells, suggesting that AFP expression may be cell line specific.

We then examined the ability of Hey-derived PGCCs to differentiate. In PGCC-derived spheroids but not in regular Hey cells, oil red staining, a marker of adipose differentiation, was observed when spheroids were cultured in adipogenesis medium (Figure 3D); blue drops indicating sulfate chondroitin, a marker of chondrogenesis, were observed when spheroids were cultured in chondrogenesis medium (Figure 3E); and scale-like osteogenin-positive signals were observed when spheroids were cultured in osteogenesis medium (Figure 3F). Expression of AFP, SMA and β -tubulin was detected when spheroids were cultured in stem cell medium (Figure 3G).

When Hey cells were cultured on a scaffold membrane, PGCCs grew mainly on the membrane surface as normal fallopian-tube-like epithelial cells, the known origin of high-grade serous carcinoma,⁴³ whereas regular Hey cells invaded into the membrane (Figure 3H). These findings demonstrated that PGCCs were capable of growing back into the normal cell of origin of ovarian cancer.

Differentiation capability of PGCCs depends on nuclear location of YAP

YAP, a critical Hippo pathway protein, is involved in the regulation of stem cells and cancer development and is responsible for cytokinesis-failure-induced activation of tumor suppressor pathway.^{44,45} We examined the role of YAP in the regulation of stemness and differentiation of PGCCs. YAP was located mainly in the cytoplasm of regular Hey cells and daughter cells but predominantly in the nuclei of PGCCs (Figures 4a and b). Treatment of PGCCs with dobutamine, which inhibits YAP nuclear translocation, abolished nuclear localization of YAP (Figure 4a). Spheroids formed by Hey-derived PGCCs differentiated into endoderm as indicated by AFP, c-Kit and CXCR4 expression (Figure 4c, upper panels), but dobutamine inhibited this differentiation, as indicated by lack of daughter cells and lack of expression of markers (Figure 4c, lower panels). Spheroids formed by Hey-derived PGCCs also differentiated into astrocyte-like cells as indicated by GFAP expression (Figure 4d, upper panels), and again, dobutamine inhibited this differentiation (Figure 4d, lower panels). GATA6, a key regulator in generation of primitive endoderm,⁴⁶ was also activated in PGCCs induced by paclitaxel or CoCl₂ (Supplementary Figure 3A), suggesting that GATA6 may be a critical mediator for early embryonic-like development in somatic cells, similar to that in the embryo. We also observed endoderm differentiation of PGCCs induced by CoCl₂ (Supplementary Figure 3B).

PGCC-derived spheroids transform into mixed germ cell tumors and carcinoma of different grades *in vivo*

To determine the nature of tumors that developed from PGCC-derived spheroids *in vivo*, we injected green fluorescence protein (GFP)-ubiquitin-labeled control Hey-cell-derived spheroids (10 000

cells) and PGCC-derived spheroids (1000 cells) collected at sD7 into the subcutis or testis of SCID (severe combined immunodeficiency) mice. All the tested spheroids formed subcutaneous or testis tumors, but PGCC-derived spheroids took significantly longer to form 1 cm tumors (60–120 days vs 30 days).

Control Hey-cell-derived spheroids formed high-grade carcinomas (Figure 5A(a)). In contrast, PGCC-derived spheroids formed a spectrum of tumors, including mixed germ cell tumor composed of dysgerminoma and embryonic carcinoma (Figures 5A(b) and A(c)), dysgerminoma with skeletal muscle differentiation (Figure 5A(d)), embryonic carcinoma (Figures 5A(e) and B(g)), embryonic carcinoma transitioned into mesenchymal morphology (Figure 5A(f)), high-grade carcinoma (Figure 5A(g)), mixed high-grade and low-grade carcinoma (Figure 5A(h)) and benign squamous cells (Figure 5A(i)). Mixed germ cell tumors were observed in (19%) mice with subcutaneous and intratesticular injections (20%) and no tumors in the control groups ($P < 0.0001$; Table 1).

To further determine the level of maturation of germ cells, we performed IHC on continuous sections. Carcinoma from control cells showed high-grade morphology, weak expression of keratin and no expression of germ cell markers SALL4 and OCT4 (Figure 5B). Dysgerminoma and embryonic carcinoma from PGCC-derived spheroids showed SALL4 staining but different levels of epithelial maturation as reflected in different intensities of cytokeratin and OCT4 staining (Figure 5B). Results of additional IHC to characterize the germ cell tumor are shown in Supplementary Figures 4A and B. We also demonstrated that germ cell tumors were derived from human, not mice, using GFP-ubiquitin-labeled cancer cells (Supplementary Figure 4C).

The above findings suggested that PGCCs were capable of differentiation into primordial germ cells and a wide spectrum of epithelial neoplasms from high-grade to benign tumors.

PGCC-derived daughter cells acquire drug resistance and mesenchymal features

To determine whether PGCC-derived daughter cells differ from parental regular cancer cells, we first analyzed the apoptotic response and sensitivity to paclitaxel. Untreated daughter cells had more polyploid cells than regular cells did (Figure 6a). Following paclitaxel treatment, the total apoptotic percentage (Q2 + Q4) was lower in daughter cells than regular cells (Figure 6b). The IC50 values for paclitaxel and vincristine were significantly higher for daughter cells than for regular cells, but the IC50 values for olaparib and topotecan did not differ between the two cell types (Figure 6c, Supplementary Table 2), demonstrating that paclitaxel-induced PGCCs can generate daughter cells chemoresistant not only to paclitaxel but also to other drugs.

The daughter cells were less invasive than the regular cancer cells (Figures 6d and e). Both PGCCs and daughter cells displayed increased expression of pan-cytokeratin, mesenchymal markers vimentin, fibronectin and N-cadherin, and epithelial–mesenchymal transition regulatory transcription factors Snail, Slug and Twist 2 and decreased expression of β -catenin (Figure 6f). Morphologic features of epithelial–mesenchymal transition were also observed in xenografts (Figure 6g). Tumors from regular cancer cells grew faster than tumors from PGCC-derived daughter cells (Figure 6g). The regular cancer-cell-derived tumors had predominantly epithelial cell morphology, whereas the daughter-cell-derived tumors had mesenchymal-shaped cells with increased heterogeneity (Figure 6g), suggesting that decreased proliferation together with acquired ability to differentiate via epithelial–mesenchymal transition confers acquired resistance to paclitaxel in daughter cells.

Formation of PGCCs and dedifferentiation of ovarian cancer after chemotherapy
 We reasoned that we should be able to observe dedifferentiation following chemotherapy in ovarian cancers in patients. Toward

this end, we examined paired specimens of human ovarian cancer obtained before and after chemotherapy. Although the pre-chemotherapy specimens had relatively homogeneous cells, the post-chemotherapy specimens had increased numbers of

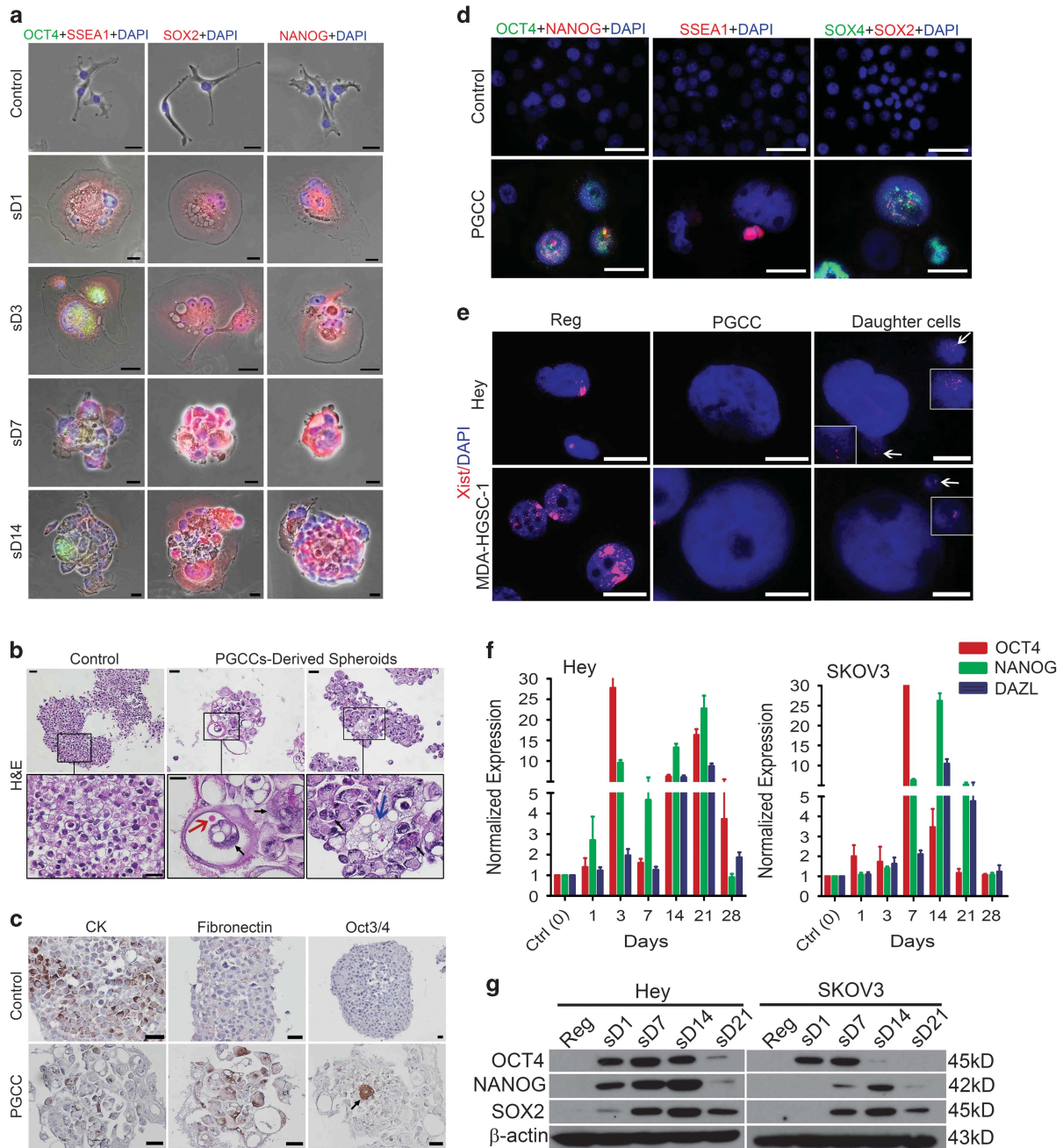


Figure 2. Generation of embryonic-like stemness of PGCCs. **(a)** Immunofluorescence photos of OCT4, SSEA1, SOX2 and NANOG in spheroids derived from Hey-derived PGCCs cultured in stem cell medium and reattached on coverslips at different time points. sD, spheroid day. Scale bars, 50 μ m. **(b)** Hematoxylin–eosin (H&E) staining of spheroids from regular Hey cells and PGCCs at sD7 in stem cell medium. Bottom panels are enlarged views of the boxed areas. Black arrow, anaplastic nuclei in a cyst; orange arrow, erythrocyte-like cell in cyst; blue arrow, macrophage-like cell. Scale bars, 50 μ m. **(c)** IHC (colored by DAB, brown) showed the expression of cytokeratin (CK), fibronectin and OCT3/4 in spheroids derived from regular Hey cells and Hey-derived PGCCs. Black arrow indicates rare positive OCT3/4 cells in the middle of spheroids. Scale bars, 50 μ m. **(d)** Immunofluorescence photos of OCT4, NANOG, SSEA1, SOX4 and SOX2 in regular MDA-HGSC-1 cells and spheroids derived from MDA-HGSC-1-derived PGCCs on recovery day 7 (sD1) in stem cell medium. Scale bars, 50 μ m. **(e)** Immunofluorescence photos of Xist in regular Hey and MDA-HGSC-1 cells, PGCCs derived from these cells, and PGCC-derived daughter cells. Boxed regions in the two daughter panels are daughter cells with high magnification, indicated by white arrowheads. Bars, 20 μ m. **(f)** Quantification of OCT4, NANOG and DAZL by qRT-PCR analysis in Hey and SKOV3 cells allowed recovering in regular medium at different times after paclitaxel treatment. **(g)** Expression of OCT4, NANOG and SOX2 in Hey- and SKOV3-derived PGCCs at different times after paclitaxel treatment, detected by western blotting.

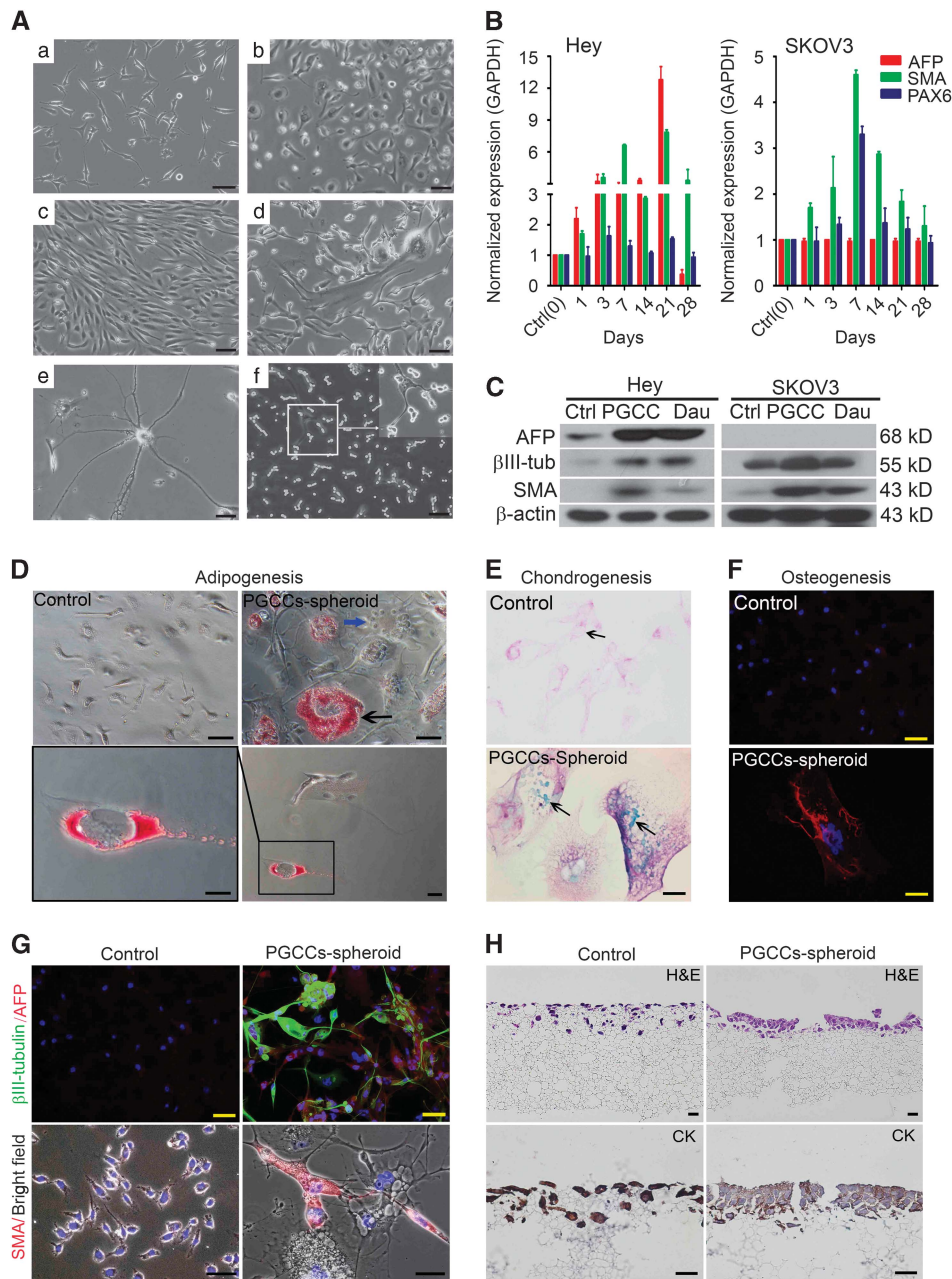


Figure 3. Differentiation of PGCCs *in vitro*. **(A)** Differentiation of PGCC to cells of different morphology at 2 months of culture in regular medium. (a) Regular Hey cells. (b–f) Daughter cells of different morphology, including epithelium-like (b), fibroblast-like (c), mixed epithelial and mesenchymal cells (d), neuron-like (e) and small spore-like cells (f). **(B)** Normalized mRNA expression of proteins associated with three germ layers in Hey-derived and SKOV3-derived PGCCs over 28 days of recovery in regular medium. AFP, SMA and PAX6 are markers for endoderm, mesoderm and ectoderm, respectively. **(C)** Expression of proteins associated with three germ layers in regular Hey and SKOV3 cells, PGCCs derived from these cells and PGCC-derived daughter cells. AFP, SMA and β 3-tubulin are markers for endoderm, mesoderm and ectoderm, respectively. Ctrl, regular cancer cell (day 0); PG, PGCC at sD1; Dau, daughter cell. **(D–F)** Adipocyte **(D)**, chondrocyte **(E)** and osteocyte **(F)** differentiation of regular Hey cells and reattached spheroids derived from PGCCs cultured in specific differentiation medium for 14 days. Black arrow in **D**, oil red–positive vesicle. Blue arrow in **D**, negative cell (internal reference). Black arrows in **E**, blue signals of sulfate chondroitin. **(G)** Immunofluorescence images of three-germ-layer differentiation of regular Hey cells and reattached spheroids from PGCCs. **(H)** 3D culture of regular Hey cells and PGCCs (at sD1) in the Alvetex scaffold system for 7 days. Regular Hey cells penetrated into the scaffold membrane, while PGCCs mainly grew on the surface of the membrane and formed a monolayer epithelial-like structure (hematoxylin–eosin (H&E) staining). Human-specific cytokeratin (CK) positivity confirmed the epithelium source.

anaplastic PGCCs with marked variation in size and large bizarre nuclei (Figures 7A and B). Post-chemotherapy specimens had small daughter cells budded off from a single PGCC (Figures 7B and C, black arrow) and erythrocyte-like cells within the cytoplasm of PGCCs (Figures 7Bd, blue arrow). The nuclear area of budded

daughter cells was significantly smaller than that of pre-chemotherapy cancer cells (Figure 7D).

After chemotherapy, 3 of 38 samples were positive for OCT4 (in cytoplasm and nuclei), 12 of 38 were positive for NANOG (mainly in cytoplasm) and 17 of 38 were positive for SOX2 (mainly in

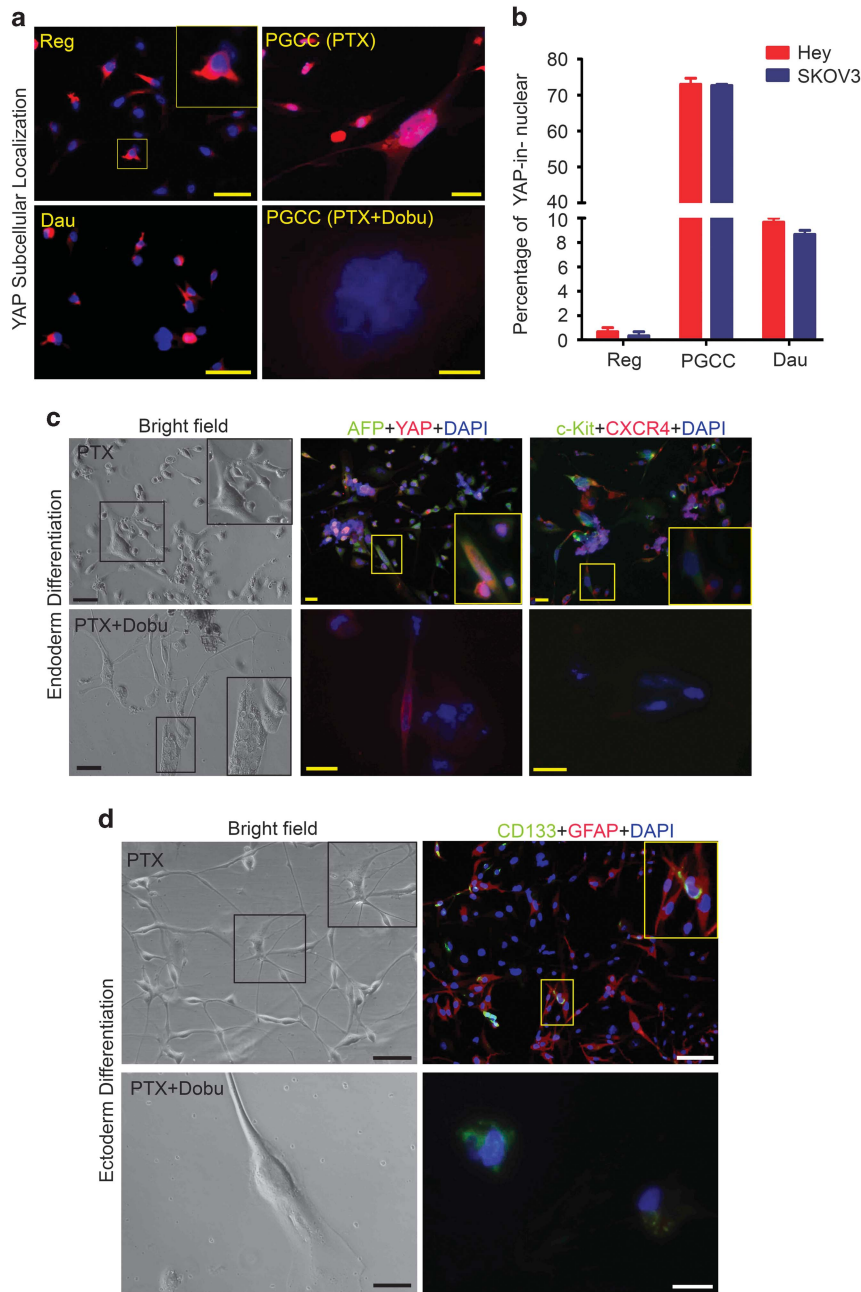


Figure 4. Subcellular localization of YAP and differentiation of PGCCs to endoderm and ectoderm (astrocytes). **(a)** Expression and distribution of YAP in test cells. In regular cells and PGCC-derived daughter cells, YAP was mainly located in the cytoplasm, but in PGCCs, YAP was predominantly located in the nucleus. Translocation of YAP to the nucleus in PGCCs could be inhibited by dobutamine (Dobu), leading to continued endoreplication and budding failure and death. **(b)** Proportion of YAP in nucleus in regular cells, PGCCs and PGCC-derived daughter cells. The proportion of YAP in the nucleus was significantly higher in PGCCs (Hey, $73.0 \pm 3.0\%$; SKOV3, $72.6 \pm 0.6\%$) and daughter cells (Hey, $9.7 \pm 0.6\%$; SKOV3, $8.6 \pm 0.6\%$) than in regular cells (Hey, $0.7 \pm 0.5\%$; SKOV3, $0.4 \pm 0.5\%$). **(c and d)** Endoderm differentiation (marked by AFP, c-Kit and CXCR4) and astrocyte differentiation (marked by GFAP and CD133) were inhibited by dobutamine (Dobu). Scale bars, 50 μm .

nuclei); before chemotherapy, no cases were positive for OCT4 or NANOG, and only 2 of 38 were positive for SOX2 (mainly in the cytoplasm; Figure 7E). Nuclear localization of YAP was observed in the three cases of post-chemotherapy not in pre-chemotherapy control (Figure 7E). These findings demonstrated that treated cancer cells showed increased expression of embryonic stem cell markers in a subset of post-chemotherapy treated ovarian cancers.

Xist expression is generally associated with differentiated state of somatic cells.⁴¹ We examined Xist expression in regular cancer cells and PGCCs. Xist was strongly expressed in nuclei of cancer

and stromal cells before chemotherapy but was largely lost in nuclei of PGCCs after chemotherapy (Figure 7F), further supporting the concept that PGCCs acquired embryonic-like stemness.

DISCUSSION

In this work, we demonstrated that PGCCs are the somatic equivalent of blastomeres. This study validated our early reports that showed embryonic-like stemness of PGCCs.^{2,14,21,22} By using CoCl_2 to induce hypoxia or paclitaxel to induce mitotic failure, we

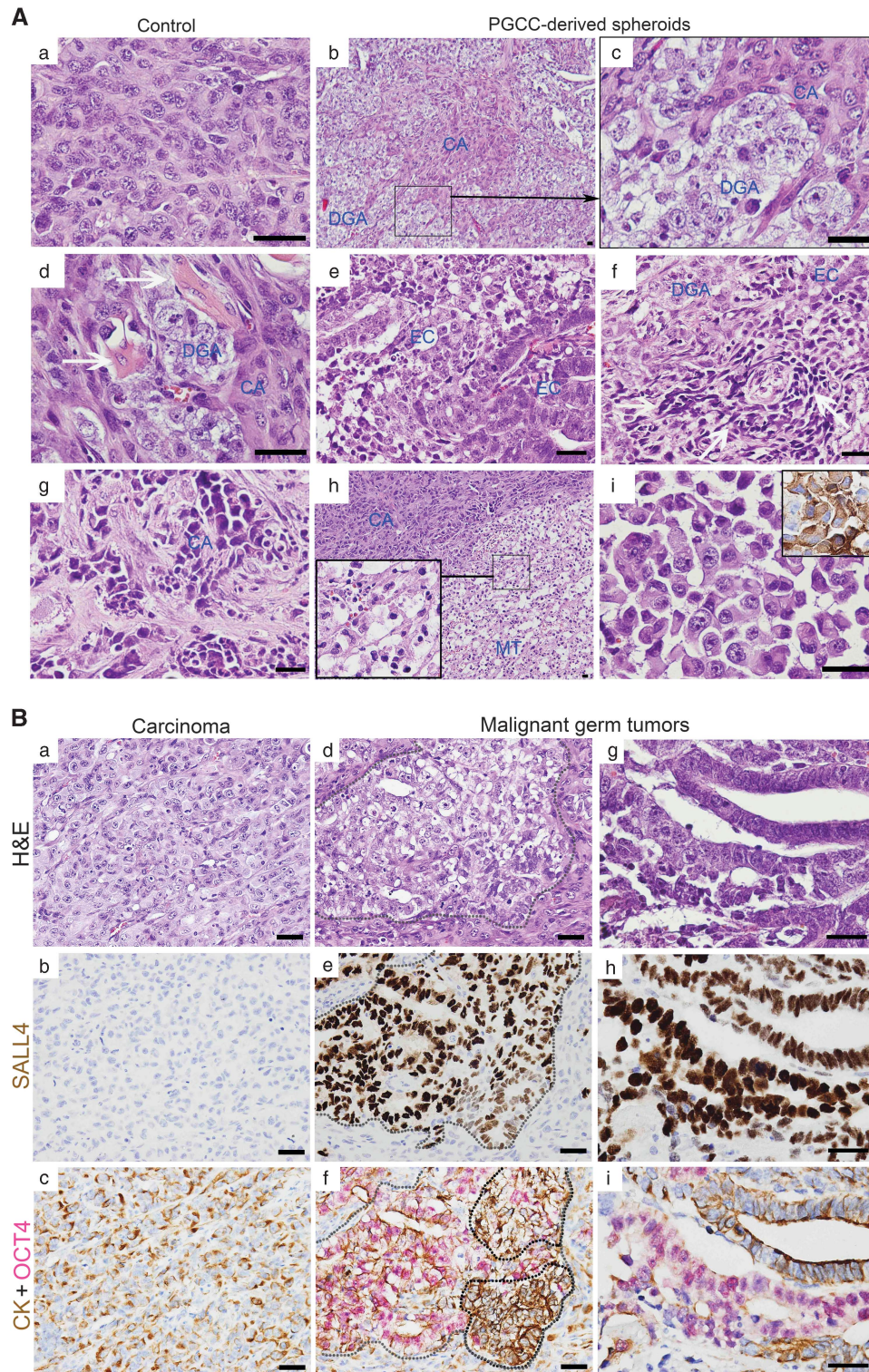


Figure 5. Formation of germ cell tumors and carcinomas of different grades from PGCC-derived spheroids. **(A)** Hematoxylin–eosin (H&E)-stained images from xenografts formed by control Hey cells and PGCC-derived spheroids. (a) control Hey cells; (b) low-power view of multiple foci of dysgerminoma in a background of carcinoma; (c) high-power view of dysgerminoma showing vesicular nuclei and clear cytoplasm of tumor cells characteristic of primordial germ cells; (d) dysgerminoma with skeletal muscle differentiation; (e) mixed dysgerminoma and embryonic carcinoma; (f) dysgerminoma with mesenchymal morphology; (g) high-grade carcinoma; (h) mixed high- and low-grade tumor with high-power view; (i) benign squamous cells with immunohistochemical staining against cytokeratin. **(B)** H&E staining and IHC for SALL4, cytokeratin (CK) and OCT4 on continuous sections of xenografts formed by regular Hey cells (Control) and malignant germ cell tumors generated from spheroids derived from PGCCs. In control xenografts formed by regular Hey cells, cancer cells were positive for human-specific CK, but not for OCT4 and SALL4. In xenografts formed by PGCC-derived spheroids, all of the cancer cells were positive for human-specific CK, and there were clusters of cells positive for OCT4 and SALL4. Gray circles show the same subpopulations. Black cycle indicates cytokeratin positive cells. Scale bars, 50 μ m.

Table 1. Frequency of tumors with different levels of differentiation in the developmental hierarchy within the xenografts inoculated with PGCC-derived spheroids in SCID mice

Group	Diagnosis	Injection site		P-value
		Subcutaneous (percentage)	Testis (percentage)	
Control	Mixed germ cell tumor	0 (0)	0 (0)	< 0.0001
	High-grade carcinoma	8 (100)	8 (100)	
PGCCs	Mixed germ cell tumor	3 (19.0)	2 (20.0)	
	Carcinoma	13 (81.0)	8 (80.0)	
	High grade	8 (50)	5 (50.0)	
	Low grade	0 (0)	0 (0)	
	High grade/low grade	5 (31.0)	3 (30.0)	

Abbreviations: PGCC, polyploid giant cancer cell; SCID, severe combined immunodeficiency.

showed that PGCCs acquired the properties of blastomeres, including differentiation into three germ layers and formation of germ cell tumors and carcinoma of different grades as well as benign tissue, similar to what have traditionally been referred as teratocarcinomas except that the tumors described here were generated via reprogramming from epithelial carcinoma cells.^{47,48} To our knowledge, PGCCs are the most primitive induced cancer stem cells reported to date.

The embryonic origin of cancer was proposed as early as the late nineteenth century by Cohnheim in 1867.⁴⁹ However, direct experimental evidence for an embryonic origin of cancer was lacking until Stevens demonstrated in 1964 that the embryonic stem cells from murine blastocysts could develop into teratoma/teratocarcinoma,^{50,51} and Pierce demonstrated in the same year that single embryonic carcinoma cells could generate multiple lineages of benign cells⁵² and in 1971 that carcinoma can generate benign cells.⁵³ This work led Pierce to propose that tumors are caricatures of the process of tissue renewal and maturation arrest.^{54,55} These early experiments clearly linked embryogenesis, tissue differentiation and tumor initiation.

More recently, the work of Nobel laureates Gurdon and Yamanaka and others has made clear that much development is a bidirectional process.^{56–58} The tumorigenicity of both embryonic stem cells and induced pluripotent stem cells is well known.^{59,60} Just as maturation arrest of differentiation can lead to tumor development, incomplete reprogramming can lead to tumor development,⁶¹ activation of embryonic program has also been shown in irradiation treated tumor cells,⁶² although it remains unknown whether there is an endogenous pathway capable of activating an embryonic program in somatic cells. Our findings reported here demonstrate that PGCCs may be a missing link that can lead to de-repression of a repressed embryonic program in somatic cancer cells for drug resistance and disease relapse.

Our findings above and in our previous publications^{2,21,22,25} prompted us to conceptualize a blastomere model for tumorigenesis and disease relapse. In normal preimplantation embryonic development (Figure 8A), after fertilization, the zygote undergoes cleavage division to generate a two- and four-cell blastomere, which can grow into polyplod blastomeres because of increased mitosis/cytokinesis failure, which undergo compaction and then develop into a morula and blastocyst. Differentiation into the inner cell mass and trophectoderm then occurs, followed by cell sorting into the primitive endoderm and pluripotent epiblasts and then gastrulation to form the three germ layers and germ cells. The stem cells differentiate along specific levels of the developmental hierarchy and become restricted to specific cell types. Maturation arrest due to genetic/epigenetic mutations acquired in embryo or later in life (M' for germ cells; M1 to M4 for somatic

cells) at the different levels of the developmental hierarchy generates tumors of different grades of malignancy, a phenomenon referred to as Pierce maturation arrest.⁵⁵

Similarly, somatic cells can enter blastomere-like development by switching mitosis to endoreplication (Figure 8B) via the giant cell cycle that we recently described.²⁵ During the initiation phase of the giant cell cycle, failed mitosis/cytokinesis activates endoreplication, by which cells can escape senescence/apoptosis. During the self-renewal phase, the polyploid cells grow autonomously and develop into compaction-, morula- and blastocyst-like embryos and generate inner cell-mass-like stem cells. During the termination phase, polyploid growth ends and the inner cell-mass-like stem cells bud small embryonic-like stem cells. During the stability phase, these stem cells with acquired genetic/epigenetic mutations that arrested at different developmental hierarchies (a', b', c' and d') will gradually acquire competence in mitosis, achieve stable diploid karyotype and grow into tumors of different grades, including germ cell tumors. The level of dedifferentiation varies according to the type of stressors and duration of stress and the cell type: the longer the giant cell cycle, the closer the resulting cells to the primitive stage and the greater level of their developmental potential for different grades as well as types of tumors.

Our findings also provide new insights into chemotherapy resistance. Paclitaxel is a microtubule poison;⁶³ its therapeutic effects are largely due to arrest of cells at mitosis, which leads to mitotic catastrophe and cancer cell death via apoptosis or necrosis or chromosomal missegregation.^{64,65} However, resistance to paclitaxel is common in patients. Polyploidy has recently been proposed to be the main cause of docetaxel resistance.⁶⁶ Our studies provide strong experimental evidence supporting a central role of polyploidy in drug resistance by providing most primitive cancer stem cells for drug resistance and disease relapse.

In summary, our findings constitute strong experimental evidence that PGCCs function as blastomere-like stem cells to facilitate the neoplastic evolution in response to various genetic/epigenetic or environmental stressors. Blocking formation of polyploidy and redirecting differentiation of PGCCs toward benign lineages may be promising therapeutic approaches for cancer.

MATERIALS AND METHODS

Cell lines, cell labeling, PGCC formation and clinical specimens

Human ovarian cancer cell lines Hey and SKOV3 were recently described.²⁵ Human MDA-HGSC-1, MD Anderson high-grade serous carcinoma cell line 1 (ID 2414), was established from a patient-derived xenograft from high-grade ovarian serous carcinoma. This line grew as spheroids in low-attachment dishes in modified medium (WIT/NoE, 1:1). The Hey cells were labeled with ubiquitin-enhanced GFP (FG12) as described previously.²⁵ At 60–70%

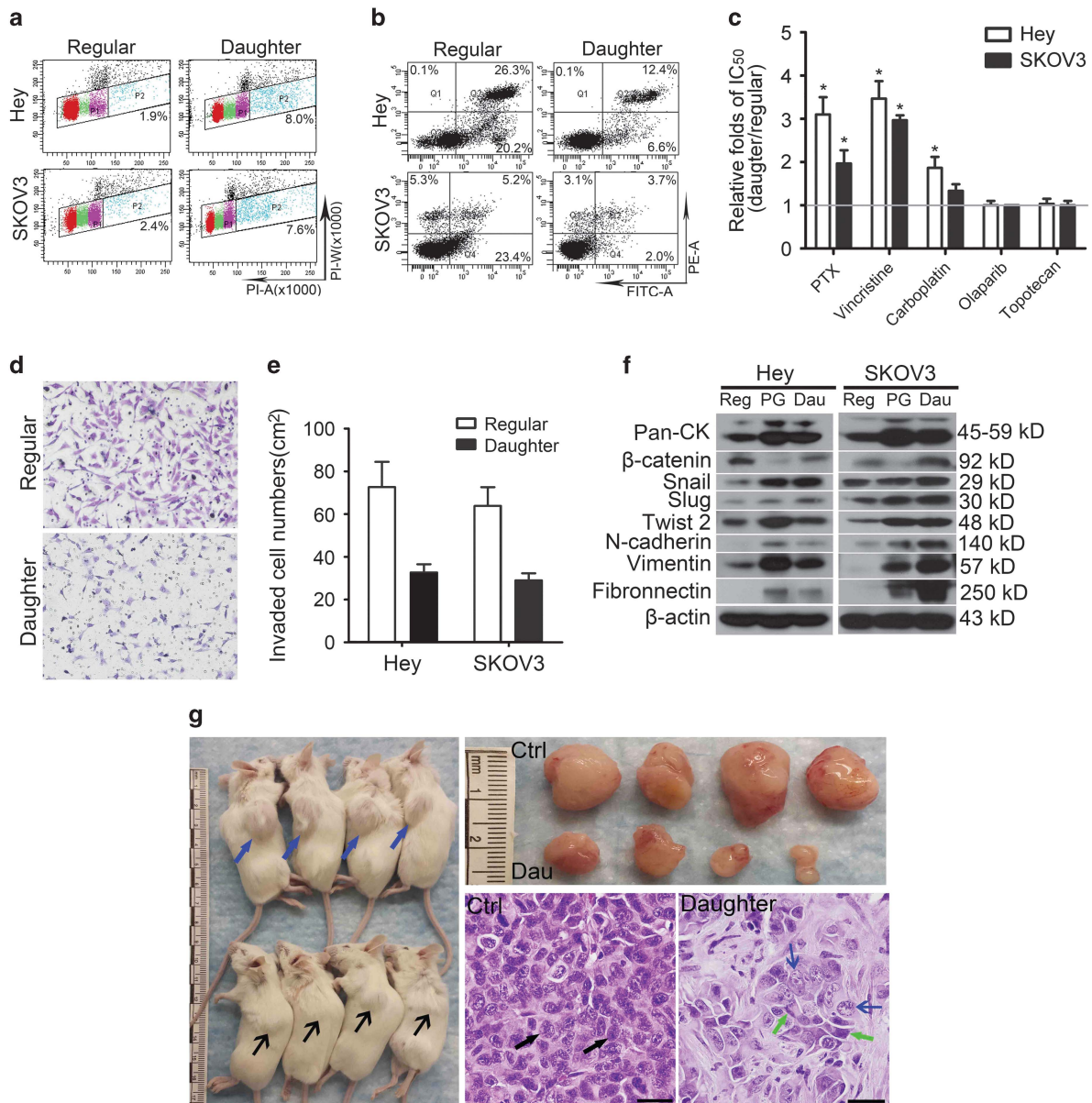


Figure 6. Acquisition of drug resistance and increased expression of epithelial and mesenchymal markers in PGCC-derived daughter cells. **(a)** Percentage of polyploid cells (blue dots in gate P2) among regular Hey and SKOV3 cells and PGCC-derived daughter cells. **(b)** Percentage of apoptotic cells (Q2+Q4) among regular Hey and SKOV3 cells and PGCC-derived daughter cells after exposure to 100 nM PTX and recovery for 48 h. **(c)** Sensitivity of PGCC-derived daughter cells compared with corresponding regular cancer cells to PTX, vincristine, carboplatin, olaparib and topotecan (24 h treatment). Results are presented as the ratio of the IC50 value for daughter cells to the IC50 value for regular cancer cells. The IC50 values are indicated in Supplementary Table 2. **(d)** and **(e)** Invasion ability of regular Hey and SKOV3 cells and PGCC-derived daughter cells. In matrigel-transwell invading experiments, the number of invaded regular Hey cells ($72.6 \pm 11.8/\text{cm}^2$) and SKOV3 cells ($63.8 \pm 8.7/\text{cm}^2$) was higher than the number of invaded daughter cells (Hey daughter, $32.7 \pm 3.8/\text{cm}^2$; SKOV3 daughter, $28.6 \pm 3.4/\text{cm}^2$). **(f)** Expression of epithelium-related and mesenchyme-related protein in tested cell lines, detected by western blotting. Reg, regular cancer cells; PG, PGCCs at day 7 after paclitaxel treatment; Dau, daughter cells. **(g)** Acquisition of mesenchymal phenotype in xenografts generated by PGCC-derived daughter cells. Left panel, tumor nodules of regular control and daughter cell groups are indicated with blue and black arrows, respectively. Right upper panel, nodule size of test groups. Right lower panels, H&E staining of xenografts. Similar-sized cancer cells in control are indicated with black arrows, and heterogeneous-size cancer cells in the daughter group are indicated with blue (epithelial-like) and green (mesenchymal-like) arrows.

confluence, the cells were treated with paclitaxel (500 nM, Sigma, St Louis, MO, USA) overnight (16–18 h); the cells were then allowed to recover for 7 days to form PGCCs.

Thirty-eight paired samples of archived, paraffin-embedded high-grade ovarian serous carcinoma obtained before and after six cycles of paclitaxel- and carboplatin-based chemotherapy were subjected to histology analysis and IHC for different markers. Use of these samples was approved by MD Anderson's Institutional Review Board.

Spheroid formation

At recovery day 7 after paclitaxel treatment, PGCCs were dissociated and cultured with FBS-free stem cell medium (Gibco, Grand island, NY, USA) in low-attachment plates (Corning, Corning, NY, USA). A total of 5000 test cells in 3 ml of stem cell medium were cultured in 60 mm low-attachment dishes. Spheroid formation was then observed for an additional 14 days. Spheroids more than 100 μm in diameter were counted. Spheroids were

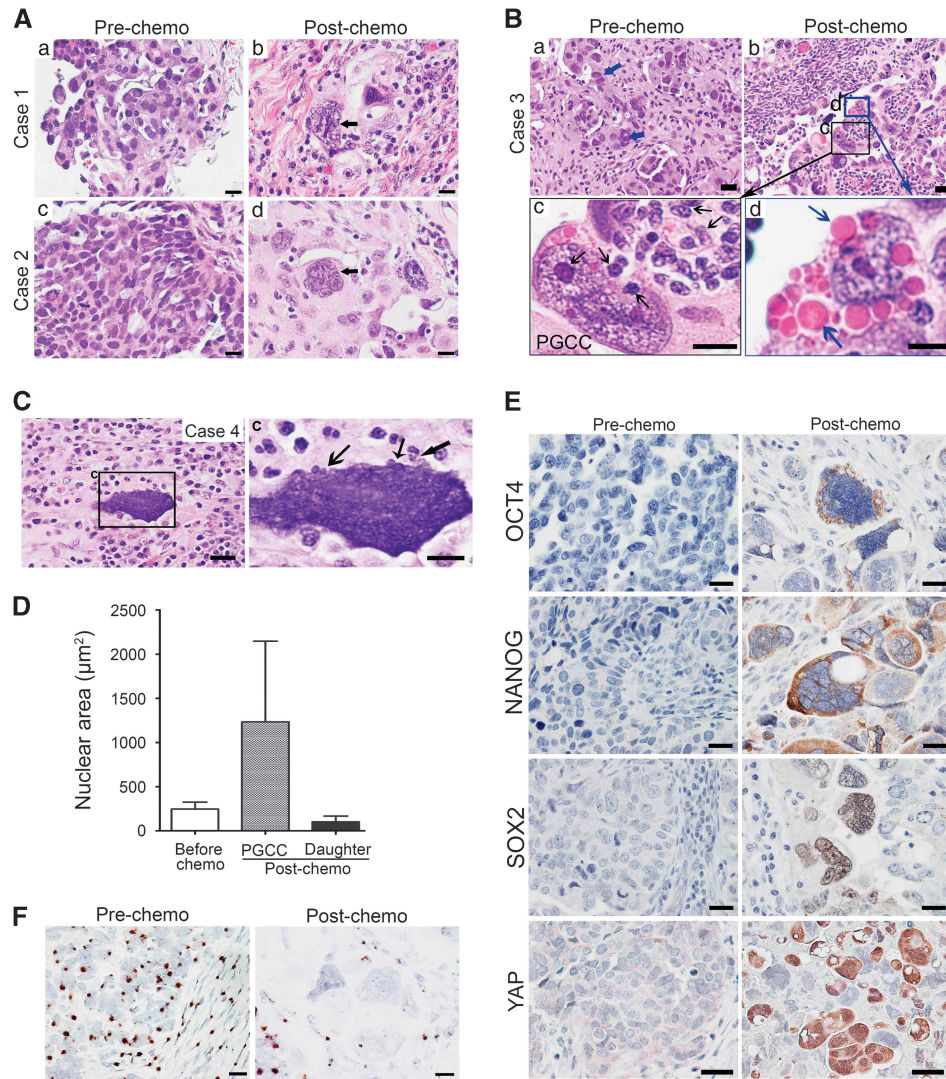


Figure 7. PGCCs and differentiation in ovarian cancer specimens. (a–c) Hematoxylin–eosin (H&E) staining shows the PGCC populations before and after chemotherapy in three paired cases. In the first two cases (A), cells in the pre-chemotherapy specimen were homogeneous in size and morphology with small round nuclei; the PGCCs (black arrows) present after chemotherapy had large bizarre nuclei and rich cytoplasm. In the third case (B), some large cancer cells were present before chemotherapy (a; blue arrows), but PGCCs present after chemotherapy (b) were larger. Some small daughter cells (black arrows) budded off from the PGCCs (c, higher magnification of b) and some erythrocyte-like vacuoles formed in the cytoplasm of PGCCs (d, higher magnification of b) and released out (blue arrows). In case 4 (C), there was prominent budding from PGCCs after chemotherapy (indicated by black arrows). (D) Nuclear area of cancer cells before chemotherapy and PGCCs and daughter cells after chemotherapy. (E) Expression of OCT4, NANOG, SOX2 and YAP in cancer cells before chemotherapy and PGCCs after chemotherapy. (F) RNA *in situ* hybridization analysis of Xist. Before chemotherapy, Xist was widely positive in most nuclei of cancer cells and stromal cells; after chemotherapy, there were fewer positive spots in the nuclei of PGCCs.

also grown from PGCCs induced by CoCl_2 as previously described;² these spheroids were used to study endoderm differentiation.

Hematoxylin–eosin staining, immunohistochemistry and immunofluorescence

Hematoxylin–eosin staining, IHC and single and double immunofluorescence labeling were performed as described previously². Primary antibodies are listed in Supplementary Table 1.

β -Gal staining

β -Gal staining for senescence was performed as described previously.⁶⁷

Western blot analysis

Western blot analysis was performed as described previously.⁶⁸

Scanning electron microscopy

Attached PGCCs, spheroids and control regular cancer cells were examined with scanning electron microscopy as previously described.⁶⁹

Live 3D confocal scanning of early-stage PGCC-derived spheroids

GFP-ubiquitin-labeled Hey cells were treated with paclitaxel, allowed to recover in regular medium for 7 days, and then cultured with stem cell medium for 2 days. The cells and spheroids were stained with Hoechst 33342 and multiply scanned at XY axis along the Z direction; images were reconstructed with a Carl Zeiss 710 confocal microscope (Zeiss, Thornwood, NY, USA).

Xist RNA *in situ* hybridization

An RNAscope immunofluorescence kit (Advanced Cell Diagnostics, Hayward, CA, USA) was used on fixed cells on coverslips and an RNAscope

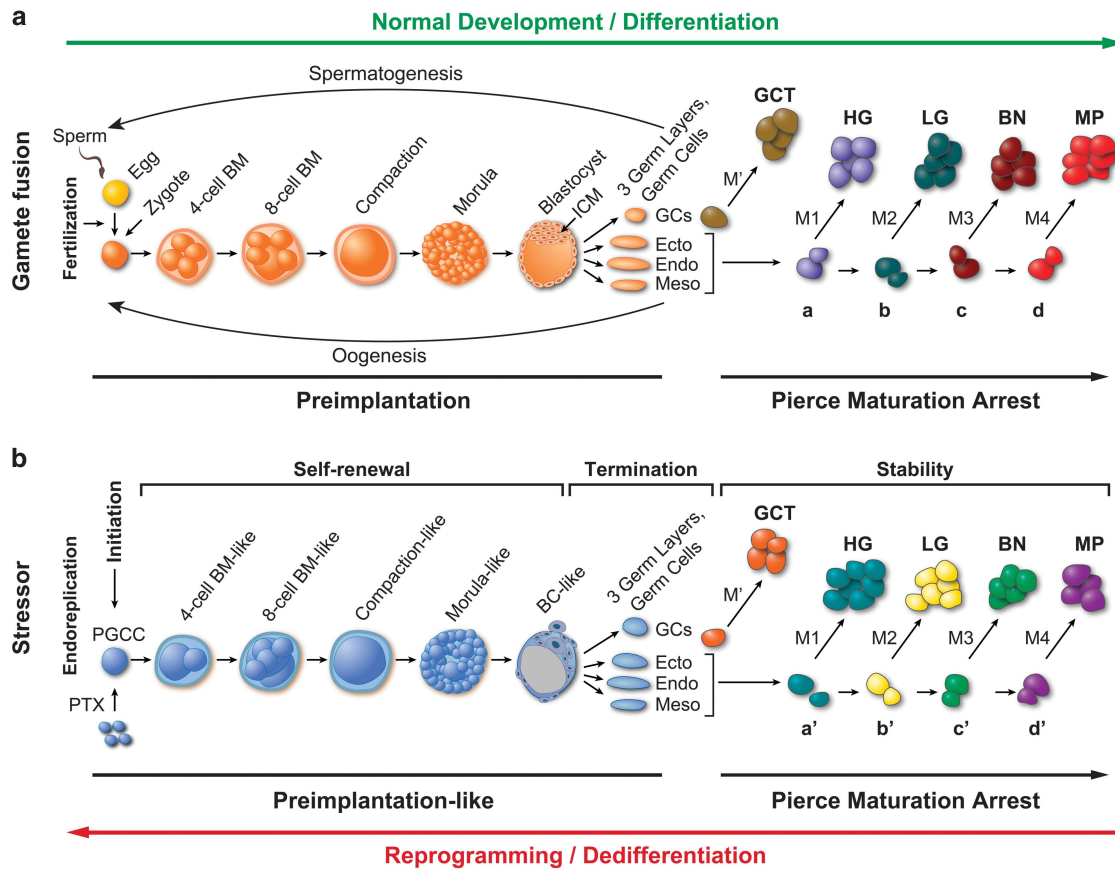


Figure 8. Schematic of blastomere model for cancer origin and disease relapse. **(A)** Blastomere-mediated embryogenesis during differentiation (normal development) and subsequent tumor formation associated with maturation arrest of stem cells in different organs during adulthood. Following gamete fusion (sex), zygote will develop into blastomeres, compaction, morula and blastocyst/ICM. Inner cell mass will develop into primordial germ cells, which will proceed with spermatogenesis (male) or oogenesis (female); while three germ layers will develop into somatic tissues containing stem cells of primitive multipotency (a), intermediate potency (b) or late oligo-potency (c) or mature stable cells (d). Maturation arrest at different developmental hierarchies leads to formation of germ cell tumors (GCTs) or germ-layer-specific tumor with different grades of malignancy: high-grade tumors (HG), low-grade tumors (LG), benign tumors (BN) or metaplasia (MP). BM, blastomere; Endo, endoderm; Ecto, ectoderm; Meso, mesoderm; GCs, germ cells; ICM, inner cell mass. M' and M represent different genetic/epigenetic mutations acquired in germ cells and somatic cells respectively during embryonic or in adult development. a, b, c, and d represent different levels of hierarchy in normal development. **(B)** Induced blastomere-like-mediated oncogenesis via dedifferentiation (reprogramming) of somatic cells. Following mitotic failure induced by paclitaxel (PTX), somatic cells initiate endoreplication to generate PGCCs, which grow into blastomere-like (BM-like), compaction-like and morula-like cell masses (self-renewal) and then differentiate into structures morphologically similar to the blastocyst with inner cell mass and then into the three germ layers and germ cell lineage (termination). The entire process mimics development of preimplantation embryo via the giant cell cycle (preimplantation-like). The germ cells and primitive stem cells arrest at different developmental hierarchies to generate germ cell tumors (GCTs) and somatic tumors with different levels of malignancy. a', b', c' and d' correspond to levels of developmental hierarchy following stress-induced reprogramming.

kit (Advanced Cell Diagnostics) on sections of human ovarian cancer according to the manufacturer's protocol.

Analysis of stemness and differentiation capacity of PGCCs

PGCCs were cultured with stem cell medium for 7 days, reattached on coverslips and cultured on Matrigel (Corning)-coated coverslips with specific differentiation media (Gibco: adipogenesis, chondrogenesis and osteogenesis differentiation media; Stem Cell Technologies (Cambridge, MA, USA): endoderm differentiation, astrocyte-inducing, differentiation and mature media) according to the manufacturers' protocols. Dobutamine (10 μ M) was used to block the nuclear accumulation of YAP. The cells were then fixed with 10% paraformaldehyde/PBS for immunofluorescence staining.

Oil red staining for fat vacuoles was performed with a lipid staining kit (Zenbio, Research Triangle Park, NC, USA) and Alcian blue staining for chondroitin was performed with an Alcian blue pH 2.5 periodic acid-Schiff staining kit (Fisher Scientific, New Kensington, PA, USA) according to the manufacturer's protocol. Immunofluorescence staining against osteogenin, AFP, CXCR4, c-Kit, YAP, GFAP, CD133, SMA and β 3-tubulin was performed as described previously.⁷⁰ Primary antibodies are listed in Supplementary Table 1.

Flow cytometry

ALDH1-FITC, CD133-PE and CD117-APC were incubated with Hey-derived PGCCs at recovery day 7 (sD1) and analyzed by a FACS Canto II flow cytometer (BD Biosciences, San Jose, CA, USA). The ovarian cancer cells stained with propidium iodide (Sigma) were also analyzed by a FACS Canto II flow cytometer.

Invasion analysis and 3D culture

Invasion assay was performed in a matrigel invasion chamber (BD Biosciences, Bedford, MA, USA) according to the manufacturer's protocol. The 3D spatial structure of control and PGCC-derived spheroids was determined with an Alvetex scaffold system (AMS Biotechnology, Cambridge, MA, USA) according to the manufacturer's protocol.

Reverse transcription and real-time quantitative PCR

Total RNA from PGCCs at different time points (days 1, 3, 7, 14, 21, 28) was extracted and purified using an RNeasy Kit (Qiagen, Dusseldorf, Germany); 1 μ g of total RNA was used for reverse transcription with Iscript Reverse Transcription Supremix (Bio-Rad, Hercules, CA, USA), and qPCR reactions were performed in

triplicate as described previously.⁷⁰ The primers for OCT4, NANOG, DAZL, AFP, SMA and PAX6 were designed as described previously.^{71,72} Changes in gene expression were calculated by using the $\Delta\Delta C_t$ method.

Tumorigenesis in mice from spheroids or daughter cells derived from single PGCCs

Spheroids derived from single PGCCs and control cells were cultured in stem cell medium for 7 days. For testis injection, single spheroids in 10 μ l of PBS were injected one spheroid per mouse into the testis of male SCID mice 2 months of age (16 injections) and controls (eight mice). Daughter cells from single PGCC-derived colonies were isolated and passaged for more than 10 generations to obtain stable populations. Then 10⁴ daughter or control cancer cells in 50 μ l of PBS and 50 μ l of Matrigel (Corning) were injected subcutaneously into the SCID mice. When tumors reached 1 cm, the mice were killed, and the tumor nodules were harvested for histology and IHC. Tumor types were diagnosed by two pathologists (JL and NN). The primary antibodies are listed in Supplementary Table 1. The use and care of mice were approved by the MD Anderson's Institutional Animal Care and Use Committee.

Statistics

The number and diameter of spheroids were assessed in randomly selected fields by light microscopy ($\times 4$) and analyzed with *t*-test or one-way analysis of variance. Relative folds of IC50 of tested drugs, diagnosis and differentiation of xenografts were analyzed with χ^2 test. Significance was defined as $P < 0.05$, and all tests were two-sided. Statistical tests were performed with SPSS software (SPSS for Windows version 22.0, SPSS Inc, Chicago, IL, USA). All quantitative results were presented as mean \pm s.d.

CONFLICT OF INTEREST

The authors declare no conflict of interest.

ACKNOWLEDGEMENTS

This work was supported in part by a multi-investigator grant from the Cancer Prevention and Research Institute of Texas (JL); a Sister Institution Grant from MD Anderson Cancer Center Global Academic Programs; and National Cancer Institute Cancer Center Support Grant CA016672, which supported the High Resolution Electron Microscopy Facility. We thank Kim Vu for image artwork and Stephanie Deming for editorial assistance. We thank many colleagues for helpful discussions. We apologize for many investigators who embraced embryonic origin of tumor or its variants over past two centuries whose work can not be cited and discussed due to space limitation.

REFERENCES

- 1 Kumar V, Abbas AK, Fausto N, Aster J. *Neoplasia. Robbins and Cotran Pathologic Basis of Disease*. Saunders Elsevier: Philadelphia, PA, USA, 2010; Chapter 7, pp 262–270.
- 2 Zhang S, Mercado-Uribe I, Xing Z, Sun B, Kuang J, Liu J. Generation of cancer stem-like cells through the formation of polyploid giant cancer cells. *Oncogene* 2014; **33**: 116–128.
- 3 Zack TI, Schumacher SE, Carter SL, Cherniack AD, Saksena G, Tabak B *et al*. Pan-cancer patterns of somatic copy number alteration. *Nat Genet* 2013; **45**: 1134–1140.
- 4 Ganem NJ, Pellman D. Limiting the proliferation of polyploid cells. *Cell* 2007; **131**: 437–440.
- 5 Munoz-Espin D, Serrano M. Cellular senescence: from physiology to pathology. *Nat Rev Mol Cell Biol* 2014; **15**: 482–496.
- 6 Ewald JA, Desotelle JA, Wilding G, Jarrard DF. Therapy-induced senescence in cancer. *J Natl Cancer Inst* 2010; **102**: 1536–1546.
- 7 Campisi J. Aging, cellular senescence, and cancer. *Annu Rev Physiol* 2013; **75**: 685–705.
- 8 Erenpreisa J, Kalejs M, Ianzini F, Kosmacek EA, Mackey MA, Emzsin D *et al*. Segregation of genomes in polyploid tumour cells following mitotic catastrophe. *Cell Biol Int* 2005; **29**: 1005–1011.
- 9 Erenpreisa JA, Cragg MS, Fringes B, Sharakhov I, Illidge TM. Release of mitotic descendants by giant cells from irradiated Burkitt's lymphoma cell line. *Cell Biol Int* 2000; **24**: 635–648.

- 10 Sundaram M, Guernsey DL, Rajaraman MM, Rajaraman R. Neosis: a novel type of cell division in cancer. *Cancer Biol Ther* 2004; **3**: 207–218.
- 11 Walen KH. Budded karyoplasts from multinucleated fibroblast cells contain centrosomes and change their morphology to mitotic cells. *Cell Biol Int* 2005; **29**: 1057–1065.
- 12 Puig PE, Guilly MN, Bouchot A, Droin N, Cathelin D, Bouyer F *et al*. Tumor cells can escape DNA-damaging cisplatin through DNA endoreduplication and reversible polyploidy. *Cell Biol Int* 2008; **32**: 1031–1043.
- 13 Leikam C, Hufnagel AL, Otto C, Murphy DJ, Muhling B, Kneitz S *et al*. *In vitro* evidence for senescent multinucleated melanocytes as a source for tumor-initiating cells. *Cell Death Dis* 2015; **6**: e1711.
- 14 Zhang S, Mercado-Uribe I, Sood A, Bast RC, Liu J. Coevolution of neoplastic epithelial cells and multilineage stroma via polyploid giant cells during immortalization and transformation of müllerian epithelial cells. *Genes Cancer* 2016; **7**: 60–72.
- 15 Weihua Z, Lin Q, Ramoth AJ, Fan D, Fidler IJ. Formation of solid tumors by a single multinucleated cancer cell. *Cancer* 2011; **117**: 4092–4099.
- 16 Fujiwara T, Bandi M, Nitta M, Ivanova EV, Bronson RT, Pellman D. Cytokinesis failure generating tetraploids promotes tumorigenesis in p53-null cells. *Nature* 2005; **437**: 1043–1047.
- 17 Davoli T, de Lange T. Telomere-driven tetraploidization occurs in human cells undergoing crisis and promotes transformation of mouse cells. *Cancer Cell* 2012; **21**: 765–776.
- 18 Wang Q, Wu PC, Dong DZ, Ivanova I, Chu E, Zeliadt S *et al*. Polyploidy road to therapy-induced cellular senescence and escape. *Int J Cancer* 2013; **132**: 1505–1515.
- 19 Mosieniak G, Sliwinska MA, Alster O, Strzeszewska A, Sunderland P, Piechota M *et al*. Polyploidy formation in doxorubicin-treated cancer cells can favor escape from senescence. *Neoplasia* 2015; **17**: 882–893.
- 20 Chakradeo S, Elmoro LW, Gewirtz DA. Is senescence reversible? *Curr Drug Targets* 2015; **17**: 460–466.
- 21 Zhang S, Mercado-Uribe I, Liu J. Generation of erythroid cells from fibroblasts and cancer cells *in vitro* and *in vivo*. *Cancer Lett* 2013; **333**: 205–212.
- 22 Zhang S, Mercado-Uribe I, Liu J. Tumor stroma and differentiated cancer cells can be originated directly from polyploid giant cancer cells induced by paclitaxel. *Int J Cancer* 2013; **134**: 508–518.
- 23 Lopez-Sanchez LM, Jimenez C, Valverde A, Hernandez V, Penarando J, Martinez A *et al*. CoCl₂, a mimic of hypoxia, induces formation of polyploid giant cells with stem characteristics in colon cancer. *PLoS One* 2014; **9**: e99143.
- 24 Braune EB, Tsoi YL, Phoon YP, Landor S, Silva Cascales H, Ramskold D *et al*. Loss of CSL unlocks a hypoxic response and enhanced tumor growth potential in breast cancer cells. *Stem Cell Rep* 2016; **6**: 643–651.
- 25 Niu N, Zhang J, Zhang N, Mercado-Uribe I, Tao F, Han Z *et al*. Linking genomic reorganization to tumor initiation via the giant cell cycle. *Oncogenesis* 2016; **5**: e281.
- 26 Zielke N, Edgar BA, DePamphilis ML. Endoreplication. *Cold Spring Harb Perspect Biol* 2013; **5**: a012948.
- 27 Fox DT, Duronio RJ. Endoreplication and polyploidy: insights into development and disease. *Development* 2013; **140**: 3–12.
- 28 Athayde Wirka K, Chen AA, Conaghan J, Ivani K, Gvakharia M, Behr B *et al*. Atypical embryo phenotypes identified by time-lapse microscopy: high prevalence and association with embryo development. *Fertil Steril* 2014; **101**: 1637–1648.e1–5.
- 29 Chavez SL, Loewke KE, Han J, Moussavi F, Colls P, Munne S *et al*. Dynamic blastomere behaviour reflects human embryo ploidy by the four-cell stage. *Nat Commun* 2012; **3**: 1251.
- 30 Hardy K, Winston RM, Handyside AH. Binucleate blastomeres in preimplantation human embryos *in vitro*: failure of cytokinesis during early cleavage. *J Reprod Fertil* 1993; **98**: 549–558.
- 31 Kligman I, Benadiva C, Alikani M, Munne S. The presence of multinucleated blastomeres in human embryos is correlated with chromosomal abnormalities. *Hum Reprod* 1996; **11**: 1492–1498.
- 32 Van Royen E, Mangelschots K, Vercruyssen M, De Neubourg D, Valkenburg M, Ryckaert G *et al*. Multinucleation in cleavage stage embryos. *Hum Reprod* 2003; **18**: 1062–1069.
- 33 Benkhalifa M, Janny L, Vye P, Malet P, Boucher D, Menezo Y. Assessment of polyploidy in human morulae and blastocysts using co-culture and fluorescent *in situ* hybridization. *Hum Reprod* 1993; **8**: 895–902.
- 34 Vanneste E, Voet T, Le Caignec C, Ampe M, Konings P, Melotte C *et al*. Chromosome instability is common in human cleavage-stage embryos. *Nat Med* 2009; **15**: 577–583.
- 35 Mertzaniidou A, Wilton L, Cheng J, Spits C, Vanneste E, Moreau Y *et al*. Microarray analysis reveals abnormal chromosomal complements in over 70% of 14 normally developing human embryos. *Hum Reprod* 2013; **28**: 256–264.
- 36 Ledbetter DH. Chaos in the embryo. *Nat Med* 2009; **15**: 490–491.

- 37 Iwata K, Yumoto K, Sugishima M, Mizoguchi C, Kai Y, Iba Y *et al*. Analysis of compaction initiation in human embryos by using time-lapse cinematography. *J Assist Reprod Genet* 2014; **31**: 421–426.
- 38 Sadler T. *Langman's Medical Embryology*, 12th edn. Lippincott Williams & Wilkins: Philadelphia, PA, USA, 2012.
- 39 Gasser RF. The Virtual Human Embryo, Carnegie Stage 2 Figures. Available at: <https://www.ehd.org/virtual-human-embryo/figures.php?stage=2>.
- 40 Rohwedel J, Guan K, Wobus AM. Induction of cellular differentiation by retinoic acid *in vitro*. *Cells, tissues, organs* 1999; **165**: 190–202.
- 41 Wutz A. Xist function: bridging chromatin and stem cells. *Trends Genet* 2007; **23**: 457–464.
- 42 Chen HH, Welling M, Bloch DB, Munoz J, Mientjes E, Chen X *et al*. DAZL limits pluripotency, differentiation, and apoptosis in developing primordial germ cells. *Stem Cell Rep* 2014; **3**: 892–904.
- 43 Kurman RJ, Shih Ie M. The dualistic model of ovarian carcinogenesis: revisited, revised, and expanded. *Am J Pathol* 2016; **186**: 733–747.
- 44 Yu FX, Zhao B, Guan KL. Hippo pathway in organ size control, tissue homeostasis, and cancer. *Cell* 2015; **163**: 811–828.
- 45 Ganem NJ, Cornils H, Chiu SY, O'Rourke KP, Arnaud J, Yimlamai D *et al*. Cytokinesis failure triggers hippo tumor suppressor pathway activation. *Cell* 2014; **158**: 833–848.
- 46 Schrode N, Saiz N, Di Talia S, Hadjantonakis AK. GATA6 levels modulate primitive endoderm cell fate choice and timing in the mouse blastocyst. *Dev Cell* 2014; **29**: 454–467.
- 47 Pierce GB. Teratocarcinoma: model for a developmental concept of cancer. *Curr Top Dev Biol* 1967; **2**: 223–246.
- 48 Andrews PW. From teratocarcinomas to embryonic stem cells. *Philos Trans R Soc Lond B Biol Sci* 2002; **357**: 405–417.
- 49 Cohnheim J. Ueber entzündung und eiterung. *Pathol Anat Klin Med* 1867; **40**: 1–79.
- 50 Stevens LC, Little CC. Spontaneous testicular teratomas in an inbred strain of mice. *Proc Natl Acad Sci USA* 1954; **40**: 1080–1087.
- 51 Stevens LC. Experimental production of testicular teratomas in mice. *Proc Natl Acad Sci USA* 1964; **52**: 654–661.
- 52 Kleinsmith LJ, Pierce GB Jr. Multipotentiality of single embryonal carcinoma cells. *Cancer Res* 1964; **24**: 1544–1551.
- 53 Pierce GB, Wallace C. Differentiation of malignant to benign cells. *Cancer Res* 1971; **31**: 127–134.
- 54 Pierce GB, Speers WC. Tumors as caricatures of the process of tissue renewal: prospects for therapy by directing differentiation. *Cancer Res* 1988; **48**: 1996–2004.
- 55 Pierce GB. The cancer cell and its control by the embryo. Rous-Whipple Award lecture. *Am J Pathol* 1983; **113**: 117–124.
- 56 Gurdon JB, Elsdale TR, Fischberg M. Sexually mature individuals of *Xenopus laevis* from the transplantation of single somatic nuclei. *Nature* 1958; **182**: 64–65.
- 57 Takahashi K, Yamanaka S. Induction of pluripotent stem cells from mouse embryonic and adult fibroblast cultures by defined factors. *Cell* 2006; **126**: 663–676.
- 58 Wilmut I, Schnieke AE, McWhir J, Kind AJ, Campbell KH. Viable offspring derived from fetal and adult mammalian cells. *Nature* 1997; **385**: 810–813.
- 59 Blum B, Benvenisty N. The tumorigenicity of human embryonic stem cells. *Adv Cancer Res* 2008; **100**: 133–158.
- 60 Lee AS, Tang C, Rao MS, Weissman IL, Wu JC. Tumorigenicity as a clinical hurdle for pluripotent stem cell therapies. *Nat Med* 2013; **19**: 998–1004.
- 61 Ohnishi K, Semi K, Yamamoto T, Shimizu M, Tanaka A, Mitsunaga K *et al*. Premature termination of reprogramming *in vivo* leads to cancer development through altered epigenetic regulation. *Cell* 2014; **156**: 663–677.
- 62 Salmina K, Jankevics E, Huna A, Perminov D, Radovica I, Klymenko T *et al*. Up-regulation of the embryonic self-renewal network through reversible polyploidy in irradiated p53-mutant tumour cells. *Exp Cell Res* 2010; **13**: 2099–2112.
- 63 Schiff PB, Fant J, Horwitz SB. Promotion of microtubule assembly *in vitro* by taxol. *Nature* 1979; **277**: 665–667.
- 64 Weaver BA, Cleveland DW. Decoding the links between mitosis, cancer, and chemotherapy: the mitotic checkpoint, adaptation, and cell death. *Cancer Cell* 2005; **8**: 7–12.
- 65 Zasadil LM, Andersen KA, Yeum D, Rocque GB, Wilke LG, Tevaarwerk AJ *et al*. Cytotoxicity of paclitaxel in breast cancer is due to chromosome missegregation on multipolar spindles. *Sci Trans Med* 2014; **6**: 229ra43.
- 66 Ogden A, Rida PC, Knudsen BS, Kucuk O, Aneja R. Docetaxel-induced polyploidization may underlie chemoresistance and disease relapse. *Cancer Lett* 2015; **367**: 89–92.
- 67 Yang G, Rosen DG, Zhang Z, Bast Jr RC, Mills GB, Colacino JA *et al*. The chemokine growth-regulated oncogene 1 (Gro-1) links RAS signaling to the senescence of stromal fibroblasts and ovarian tumorigenesis. *Proc Natl Acad Sci USA* 2006; **103**: 16472–16477.
- 68 Liu G, Yang G, Chang B, Mercado-Urbe I, Huang M, Zheng J *et al*. Stanniocalcin 1 and ovarian tumorigenesis. *J Natl Cancer Inst* 2010; **102**: 812–827.
- 69 Szajnik M, Derbis M, Lach M, Patalas P, Michalak M, Drzewiecka H *et al*. Exosomes in plasma of patients with ovarian carcinoma: potential biomarkers of tumor progression and response to therapy. *Gynecol Obstet (Sunnyvale)* 2013; Suppl 4: 3.
- 70 Niu N, Zhang J, Sun Y, Wang S, Sun Y, Korteweg C *et al*. Expression and distribution of immunoglobulin G and its receptors in an immune privileged site: the eye. *Cell Mol Life Sci* 2011; **68**: 2481–2492.
- 71 Kamiyama T, Takahashi M, Nakagawa T, Nakanishi K, Kamachi H, Suzuki T *et al*. AFP mRNA detected in bone marrow by real-time quantitative RT-PCR analysis predicts survival and recurrence after curative hepatectomy for hepatocellular carcinoma. *Ann Surg* 2006; **244**: 451–463.
- 72 Forsdahl S, Kiselev Y, Hogseth R, Mjelle JE, Mikkola I. Pax6 regulates the expression of Dkk3 in murine and human cell lines, and altered responses to Wnt signaling are shown in Flpln-3T3 cells stably expressing either the Pax6 or the Pax6(5a) isoform. *PLoS One* 2014; **9**: e102559.



This work is licensed under a Creative Commons Attribution-NonCommercial-ShareAlike 4.0 International License. The images or other third party material in this article are included in the article's Creative Commons license, unless indicated otherwise in the credit line; if the material is not included under the Creative Commons license, users will need to obtain permission from the license holder to reproduce the material. To view a copy of this license, visit <http://creativecommons.org/licenses/by-nc-sa/4.0/>

© The Author(s) 2017

Supplementary Information accompanies this paper on the Oncogene website (<http://www.nature.com/onc>)